catalysts

Supplementary Information: Influence of Biochar Composition and Source Material on Catalytic Performance: The Carboxylation of Glycerol with CO2 as a Case Study

Catherine Collett [1], Ondřej Mašek [2], Nurul Razali [1,§] and James McGregor [1,*]

[1] Department of Chemical and Biological Engineering, University of Sheffield, Mappin Street, Sheffield S1 3JD, United Kingdom; catherine.collett@nottingham.ac.uk (C.C.), nrazali01@gmail.com (N.R.)
[2] UK Biochar Research Centre, School of Geosciences, University of Edinburgh, Edinburgh EH9 3JN, United Kingdom; ondrej.masek@ed.ac.uk
* Correspondence: james.mcgregor@sheffield.ac.uk; Tel.: +44 (0)114 222 4918

§ Present address: Faculty of Ocean Engineering Technology and Informatics, Universiti Malaysia Terengganu, 21300 Kuala Terengganu, Terengganu, Malaysia

Received: 17 August 2020; Accepted: 11 September 2020; Published: date

Raw data used to plot figures can be found in the online data repository: 10.15131/shef.data.12783941.

1. Raman Spectra – Data Collection Protocol

A Renishaw inVia Raman microscope was used in this experiment. A silicon wafer was used as a calibration source (Renishaw Raman Calibration Source). The samples were analysed in powder form. To prepare the samples, a small amount of powder was squeezed between two glass slides. One slide was then removed, leaving a reasonably flat surface for Raman analysis. Three different but representative areas were chosen for Raman analysis for each sample. This meant the non-homogeneous nature of the sample could be accounted for. The microscope magnification used was 50×. The settings used for obtaining the Raman spectra are given in Table S1 for reference.

Table S1. Settings used for obtaining Raman spectra of biochars.

Laser wavelength/nm	514
Laser power (at 100%)/mW	20
Laser intensity	1%
Number of accumulations	5
Raman Shift range/cm^{-1}	400–4000

Cosmic Ray Removal was used to mitigate the effect of random atmospheric disturbances, which can create additional intense peaks in the Raman spectra. In Cosmic Ray Removal, three spectra are obtained and the median value for each Raman shift is recorded. This removes the possibility of extreme values appearing in the final spectra. Raman spectroscopy was also carried out in a dark room, with no lights on and the computer monitor switched off, in order to avoid peaks associated with these light sources. (The example provided for SWB-550 in Figure S1 includes an example of a peak from an artificial light source.)

2. Raman Curve Deconvolution

Raman spectroscopy is commonly used for quantifying the degree of graphiticity in carbonaceous samples, by detecting graphitic and disordered carbon bands that are IR-inactive. However, no standard exists for the curve deconvolution of carbonaceous samples; methods for analysing carbon films range from fitting 2 to 11 peaks [1,2], and for biochars, between 2 and 10 peaks

[3–6]. Using a principle of a least curves fit, six peaks were fitted using Renishaw's WiRE software. The band assignments are summarised in Table S2, and are based on those identified in the literature sources. Example deconvolved spectra for SWP 550 and AC are presented in Figure S1. Raw data and details on the curve fitting parameters (width, height, area, centre) are provided in Supplementary Information repository file 10.15131/shef.data.12783941.

Table S2. Raman curve deconvolution, peak assignments.

Band name	Raman shift/cm^{-1}	Band interpretation
G_L	1700	Carbonyl group C=O
D2	1620	Graphitic lattice mode; lattice vibration involving graphene layers at surface of graphite crystal. Stretching vibrations of double bonds/olefins.
G	1580	Graphite; aromatic ring quadrant breathing; alkene C=C. In-plane C=C aromatic ring stretching.
V_L	1465	Methylene or methyl; semi-circle breathing of aromatic rings; amorphous carbon structures
D1	1350	Disordered carbon lattice vibration mode (in-plane vibrations of C=C at edge of graphene layer)
D4	1200	C-C and C=C stretching vibration of polyene-like structures.

(a)

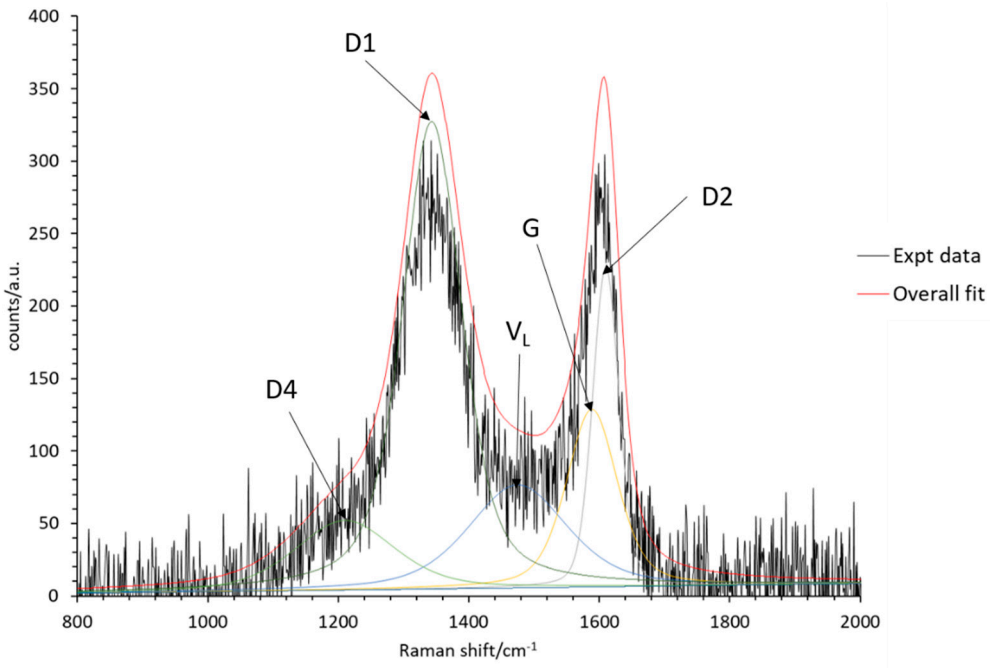

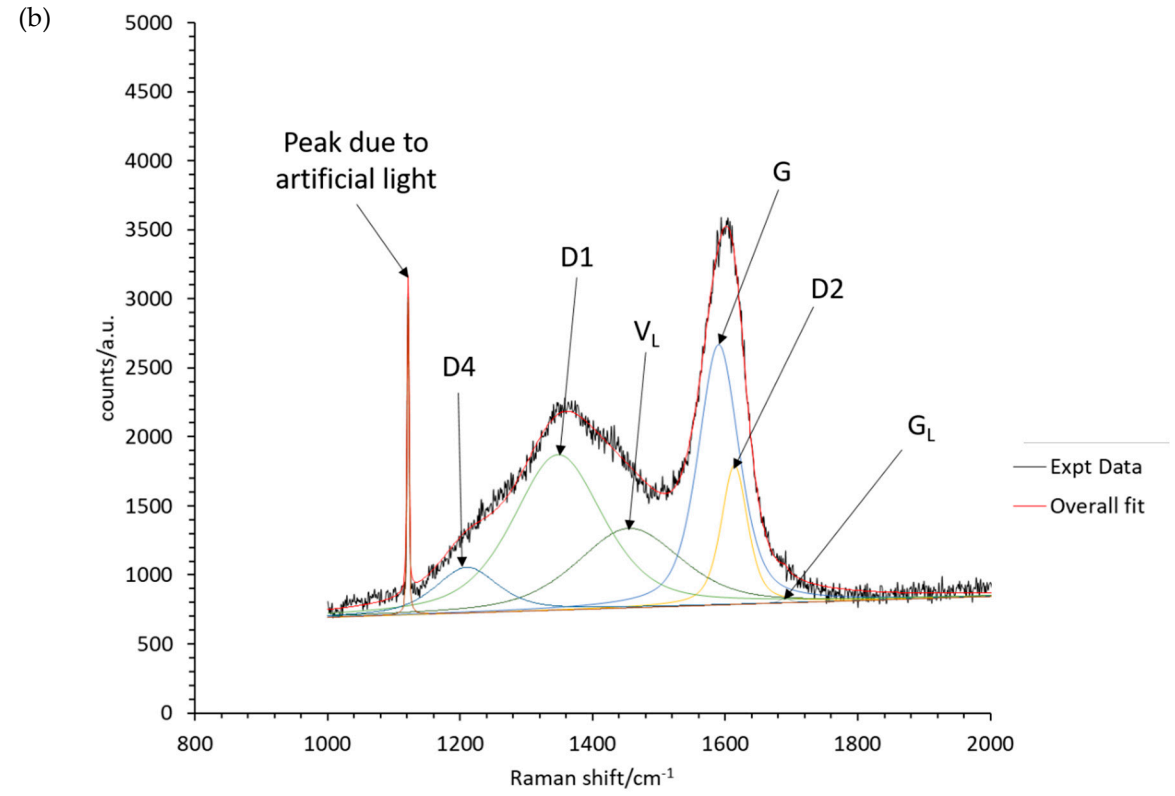

Figure S1. Deconvolved Raman spectra using a principle of a least-curves fit. (**a**) spectra for AC, note there was no evidence of a GL peak. (**b**) spectra for SWP 550.

3. FTIR Spectra (Ash and Demineralised Samples)

FTIR-ATR spectra are shown for biochars before and after demineralisation in Figure S2. The spectra from biochars and their ashes are compared in Figure S3. The FTIR-ATR spectra for biochar ash from untreated and demineralised samples are compared in Figure S4. The spectra demonstrate that there were no substantial changes to the functional groups present in the biochars as a result of demineralisation. The spectra in Figure S3 assisted with the identification of the functional groups responsible for the bands, i.e., which were due to carbon and which were due to ash content. All spectra are offset for clarity.

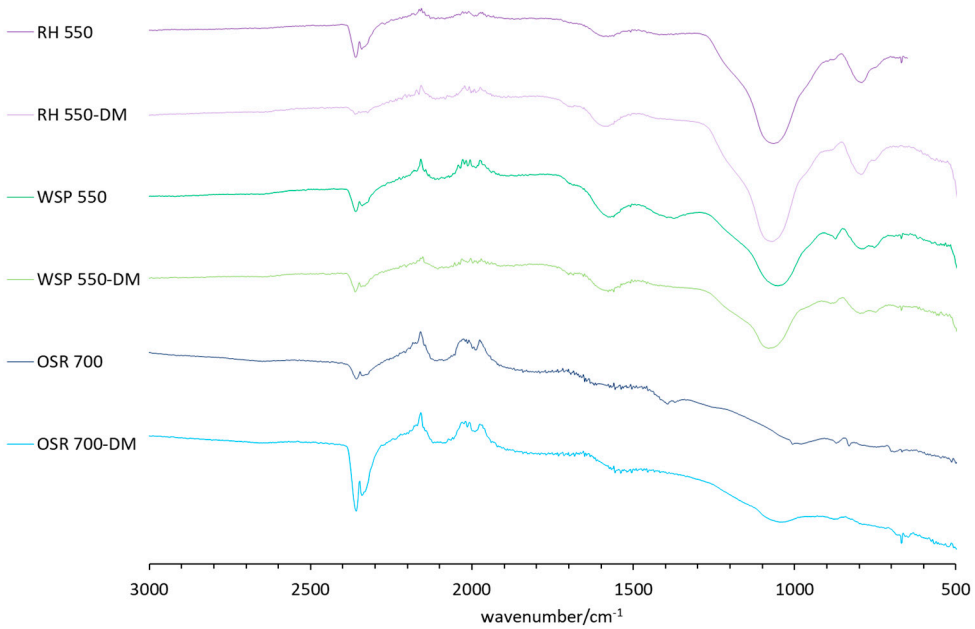

Figure S2. FTIR-ATR spectra for biochars before and after demineralisation treatment with hydrochloric acid (treated samples denoted by –DM suffix). Spectra offset for clarity.

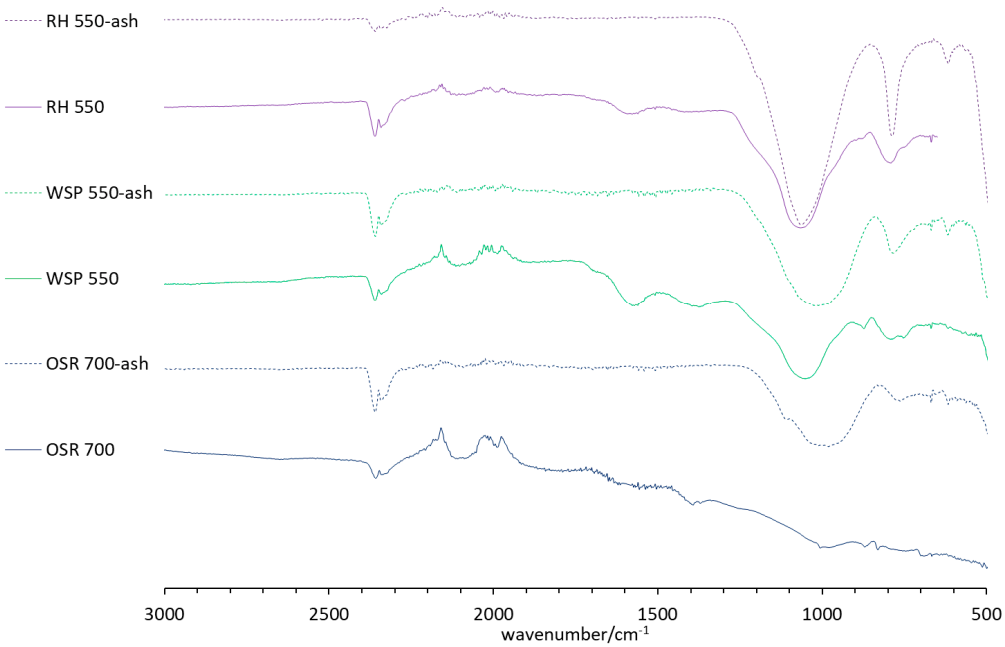

Figure S3. FTIR-ATR spectra comparing biochars and their ashes. Spectra offset for clarity.

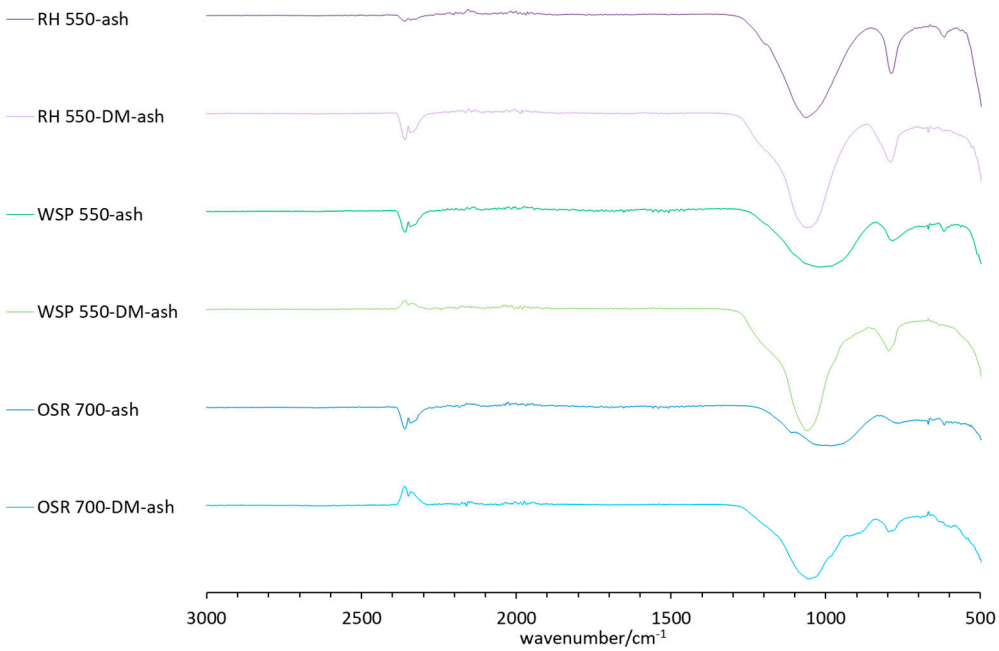

Figure S4. FTIR-ATR spectra for biochar ashes before and after demineralisation treatment with hydrochloric acid (treated samples denoted by –DM suffix). Spectra offset for clarity.

4. Calibration Protocol and Details

Calibration samples were prepared by dissolving a mixture of glycerol, glycerol carbonate (4-hydroxymethyl-1,3-dioxolan-2-one, 90% purity, Acros Organics), glycerol mono- and di-acetins (50% diacetin, Sigma-Aldrich), and glycerol triacetin (99% purity, Alfa Aesar) in ethanol. For calibration samples, the glycerol concentrations ranged from 0.1–0.01 g ml^{-1}, and glycerol carbonate and acetin concentrations ranged from 0.0005–0.01 g ml^{-1}. At least three different concentrations of calibration mixture were prepared for each calibration. Example calibration concentrations are shown in Table S3. Fresh calibration samples were prepared for each set of reactions, as it is expected that the retention times and sensitivity of the column will vary over time due to column aging.

Table S3. Calibration samples prepared for glycerol upgrading reactions in February 2018.

Sample Composition				Sample Concentration				
Vol. EtOH/ ml	**Glycerol/g**	**Glycerol carbonate /µL**	**Acetins/ µL**	**Glycerol/g ml^{-1}**	**Glycerol carbonate/g ml^{-1}**	**Monoacetin/g ml^{-1}**	**Diacetin/g ml^{-1}**	**Triacetin/g ml^{-1}**
10	1.20	70	240	0.1070	0.008694	0.005251	0.012455	0.007204
10	0.95	55	180	0.0865	0.007127	0.004036	0.009573	0.005537
10	0.70	35	120	0.0661	0.004701	0.002761	0.006548	0.003787
10	0.45	20	65	0.0431	0.002679	0.001557	0.003694	0.002136
10	0.20	4	10	0.0210	0.00055	0.000242	0.000575	0.000332

Example calibration curves are shown in Figures S5–S9 for the products of glycerol upgrading reactions from February 2018. Calibrations are presented with and without normalisation using an internal standard, 1-hexanol. 1 µl of 1-hexanol was used as an internal standard. In almost all cases,

higher R^2 values were obtained in the absence of an internal standard; this was attributed to the high retention rates of glycerol in the INNOWax column. Therefore the calibration constants without internal standard were used.

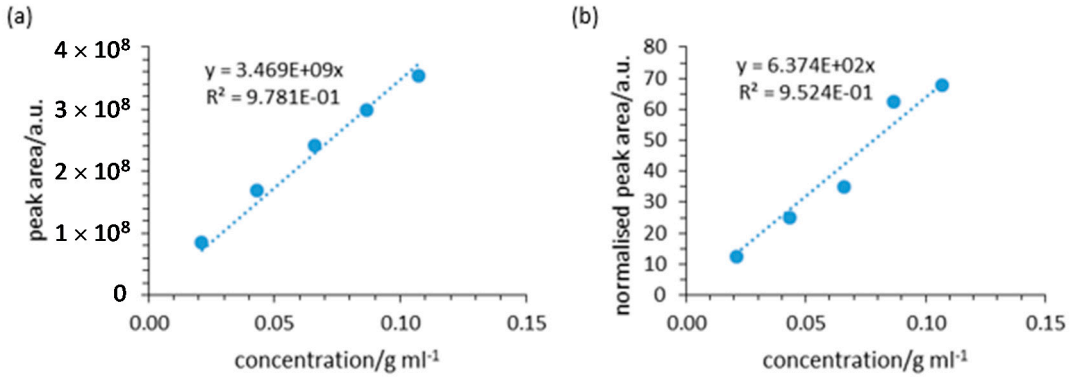

Figure S5. Calibration curves for glycerol, (**a**) without normalisation and (**b**) normalised relative to the area of the internal standard peak.

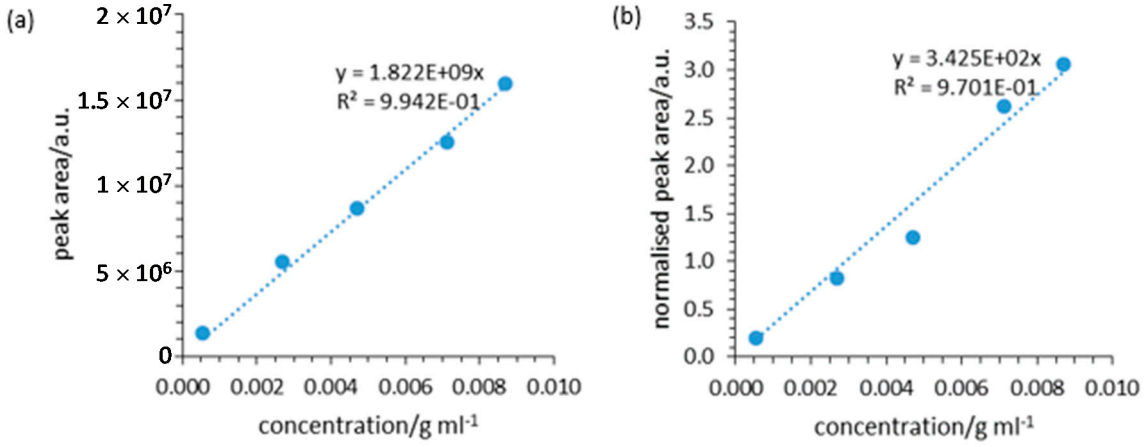

Figure S6. Calibration curves for glycerol carbonate, (**a**) without normalisation and (**b**) normalised relative to the area of the internal standard peak.

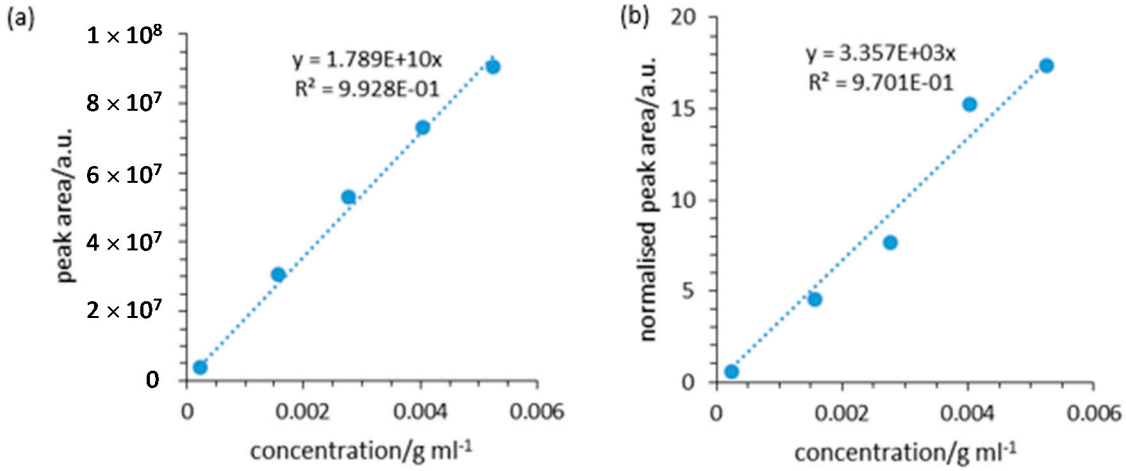

Figure S7. Calibration curves for glycerol monoacetin (**a**) without normalisation and (**b**) normalised relative to the area of the internal standard peak.

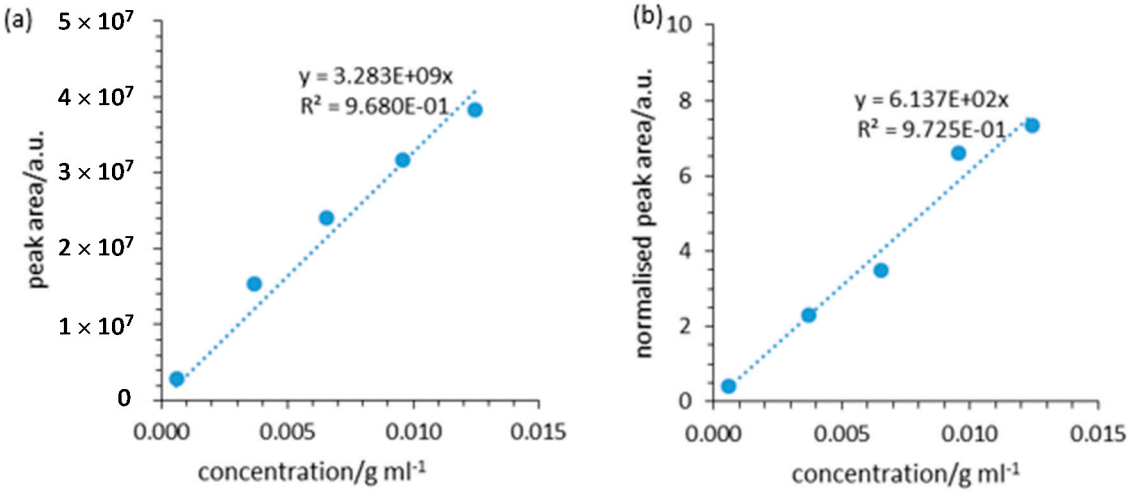

Figure S8. Calibration curves for glycerol diacetin (**a**) without normalisation and (**b**) normalised relative to the area of the internal standard peak.

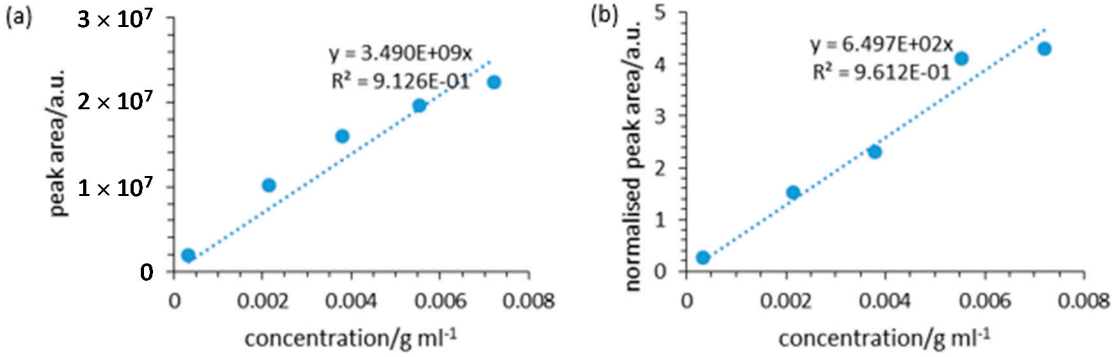

Figure S9. Calibration curves for glycerol triacetin (**a**) without normalisation and (**b**) normalised relative to the area of the internal standard peak.

The percentage error in the quantity of each product of glycerol upgrading was calculated using three repeats of OSR 550, shown in Table S4.

Table S4. Product concentrations from three repeats of OSB-550, used to calculate the percentage error.

	Concentration/mol l^{-1}				
Catalyst	Glycerol	Glycerol carbonate	Monoacetin	Diacetin	Triacetin
OSR 550 rpt1	0.2562	0.0329	0.0980	0.0188	0.0006
OSR 550 rpt2	0.3285	0.0257	0.1479	0.0325	0.0013
OSR 550 rpt3	0.5575	0.0436	0.1030	0.0027	0.0002
Average (μ)	0.3807	0.0340	0.1163	0.0180	0.0007
Standard deviation (σ)	0.1573	0.0090	0.0275	0.0149	0.0006
% error (=σ/μ)	41.3%	26.4%	23.6%	82.9%	78.1%

One complication was that pure calibration samples were unavailable for monoacetin and diacetin. The composition of the diacetin sample therefore had to be calculated. This was achieved by comparing calibrations for a pure triacetin sample with the concentration of triacetin in a 50% diacetin sample. By comparing with a 99+% triacetin sample, the composition of the acetin sample by weight was estimated to be 50 wt% diacetins, 28.9 wt% triacetin, and 21.2 wt% monoacetin (and other trace acetins). There may be a significant contribution from other acetins, such 1,2-propanediol diacetate, however precise quantification of the acetin mixture was beyond the scope of the present work. More important was quantitative comparison of the trends in acetin production between biochars, and accurate calibration of diacetin and triacetin, which were only produced in the presence of a catalyst.

References

1. Ayala, P.; Maia da Costa, M.E.H.; Prioli, R.; Freire, F.L. Nano- and micro-scale wear of fluorinated carbon films. *Surf. Coatings Technol.* **2004**, *182*, 335–341, doi:10.1016/j.surfcoat.2003.08.075.
2. Tarrant, R.N.; McKenzie, D.R.; Bilek, M.M.M. Raman characterisation of PIII multilayer carbon films. *Diam. Relat. Mater.* **2004**, *13*, 1422–1426, doi:10.1016/j.diamond.2004.01.028.
3. Zhao, L.; Cao, X.; Masek, O.; Zimmerman, A. Heterogeneity of biochar properties as a function of feedstock and production temperatures. *J. Hazard. Mater.* **2013**, 256–257, 1–9.
4. Zhao, Y.; Feng, D.; Zhang, Y.; Huang, Y.; Sun, S. Effect of pyrolysis temperature on char structure and chemical speciation of alkali and alkaline earth metallic species in biochar. *Fuel Process. Technol.* **2016**, *141*, 54–60, doi:10.1016/j.fuproc.2015.06.029.
5. Li, X.; Hayashi, J.; Li, C. Volatilisation and catalytic effects of alkali and alkaline earth metallic species during the pyrolysis and gasification of Victorian brown coal. Part VII. Raman spectroscopic study on the changes in char structure during the catalytic gasification in air. *Fuel* **2006**, *85*, 1509–1517, doi:10.1016/j.fuel.2006.01.011.
6. Chia, C.H.; Gong, B.; Joseph, S.D.; Marjo, C.E.; Munroe, P.; Rich, A.M. Imaging of mineral-enriched biochar by FTIR, Raman and SEM–EDX. *Vib. Spectrosc.* **2012**, *62*, 248–257, doi:10.1016/j.vibspec.2012.06.006.